



HAL
open science

Advances in characterization of the soil clay mineralogy using X-ray diffraction: from decomposition to profile fitting

Fabien Hubert, Laurent Caner, Alain Meunier, Bruno Lanson

► To cite this version:

Fabien Hubert, Laurent Caner, Alain Meunier, Bruno Lanson. Advances in characterization of the soil clay mineralogy using X-ray diffraction: from decomposition to profile fitting. *European Journal of Soil Science*, 2009, 60, pp.1093-1105. 10.1111/j.1365-2389.2009.01194.x . insu-00433245

HAL Id: insu-00433245

<https://insu.hal.science/insu-00433245v1>

Submitted on 18 Nov 2009

HAL is a multi-disciplinary open access archive for the deposit and dissemination of scientific research documents, whether they are published or not. The documents may come from teaching and research institutions in France or abroad, or from public or private research centers.

L'archive ouverte pluridisciplinaire **HAL**, est destinée au dépôt et à la diffusion de documents scientifiques de niveau recherche, publiés ou non, émanant des établissements d'enseignement et de recherche français ou étrangers, des laboratoires publics ou privés.

1 **Advances in characterization of the soil clay mineralogy using X-ray**
2 **diffraction: from decomposition to profile fitting**

3

4 F. HUBERT^a, L. CANER^a, A. MEUNIER^a & B. LANSON^b

5

6 ^a*HydrASA, University of Poitiers, INSU-CNRS, 40 avenue du Recteur Pineau, F-86022*
7 *Poitiers cedex, France and* ^b*Mineralogy & Environments Group, LGCA, Maison des*
8 *GéoSciences, Grenoble University, CNRS, F-38041 Grenoble Cedex 9, France.*

9

10 *Running head: Advances in soil clay mineral characterization*

11

12 *Correspondence: F. Hubert. E-mail: fhubert@etu.univ-poitiers.fr*

13 **Summary**

14 Structural characterization of soil clay minerals often remains limited despite their key
15 influence on soil properties. In soils, complex clay parageneses result from the
16 coexistence of clay species with contrasting particle sizes and crystal-chemistry and
17 from the profusion of mixed layers with variable compositions. The present study
18 aimed at characterizing the mineralogy and crystal chemistry of the $< 2 \mu\text{m}$ fraction
19 along a profile typical of soils from Western Europe and North America (Neo Luvisol).
20 X-ray diffraction (XRD) patterns were interpreted using i) the combination of XRD
21 pattern decomposition and indirect identification from peak positions commonly applied
22 in soil science and ii) the multi-specimen method. This latter approach implies direct
23 XRD profile fitting and has recently led to significant improvements in the structural
24 characterization of clay minerals in diagenetic and hydrothermal environments. In
25 contrast to the usual approach, the multi-specimen method allowed the complete
26 structural characterization of complex clay parageneses encountered in soils together
27 with the quantitative analysis of their mineralogy. Throughout the profile, the clay
28 paragenesis of the studied Neo Luvisol systematically includes discrete smectite, illite
29 and kaolinite in addition to randomly interstratified illite-smectite and chlorite-smectite.
30 Structural characteristics of the different clay minerals, including the composition of
31 mixed layers, did not vary significantly with depth and are thus indicative of the parent
32 material. The relative proportion of the $< 2 \mu\text{m}$ fraction increased with increasing depth
33 simultaneously with smectite relative proportion. These results are consistent with the
34 leaching process described for Luvisols in the literature.

35 **Introduction**

36 The $< 2 \mu\text{m}$ fraction of soils is commonly dominated by clay minerals which control, to
37 a large extent, important soil chemical and physical properties such as cation exchange
38 capacity and surface area (Dixon & Weed, 1989). In addition, clay minerals record the
39 pedogenetic history of soils (see the review of Wilson, 1999). An accurate
40 determination of clay mineralogy and of its changes along the soil profile is thus
41 essential for both purposes. Two main factors impede such a precise identification: first,
42 soil clay parageneses are most often mixtures of clay species with a variety of particle
43 sizes (50 nm – 5 μm), and crystal-chemistry. Second, soil clay minerals are often mixed
44 layers with variable compositions (Righi & Elsass, 1996).

45 Over the last decade, the combined use of DecompXR (Lanson, 1997) and Newmod
46 (Reynolds, 1985) has improved the interpretation of X-ray diffraction (XRD) patterns in
47 soils. DecompXR allows the decomposition of complex diffraction maxima into
48 elementary peaks characterized by their positions, full width at half maximum intensity
49 (FWHM) and intensities. This approach thus reveals the phase heterogeneity of samples
50 and allows quantifying compositional changes within a series of samples, for example
51 in a soil profile. However, the decomposition by itself does not allow the identification
52 of mixed layers that is the determination of the different layer types coexisting within
53 crystallites, of their proportion and stacking sequences. Mixed layer identification is
54 routinely performed from the comparison of experimental peak positions with those
55 calculated, commonly using Newmod, for mixed layers whose composition (nature and
56 proportion of the different layer types) and stacking parameters are optimized.

57 Such a combination of XRD pattern decomposition and Newmod calculations has
58 been successfully applied to samples from diagenetic or hydrothermal geological
59 settings (Lanson & Besson, 1992). It has been for soils to i) evaluate the effect of time

60 on soil formation (Righi & Meunier, 1991; Righi *et al.*, 1995; Hardy *et al.*, 1999; Egli *et*
61 *al.*, 2001, 2008; Velde *et al.*, 2003; Vingiani *et al.*, 2004; Montagne *et al.*, 2008), ii)
62 investigate the role of vegetation cover (Barré *et al.*, 2007a) and of macrofauna (Jouquet
63 *et al.*, 2007) on clay mineralogy, and iii) characterize the interactions between clay
64 minerals and organic matter in relation to carbon sequestration (Fontaine *et al.*,
65 2007). However, this dual procedure allows only an approximate characterization of the
66 mixed layers as the identification relies essentially on peak position without fitting the
67 complete reflection profiles including asymmetries and shoulders. Consistently, profile
68 fitting results in a more reliable identification of mixed layers (Drits, 2003). Fitting
69 simultaneously the profiles of various basal reflections provides additional constraints.

70 To overcome the intrinsic limitations of the previous approaches, the profile fitting
71 method calculates a complete XRD pattern from a structural model optimized for each
72 clay species present (Drits & Sakharov, 1976; Drits & Tchoubar, 1990). Drits *et al.*
73 (1997a) and Sakharov *et al.* (1999a,b) further improved the approach as several
74 structural models may fit a given experimental pattern equally well. In the multi-
75 specimen method, the optimized structural model should describe all XRD patterns
76 obtained for a given sample following different treatments such as saturation by
77 different interlayer cations, ethylene glycol solvation, heating, etc equally well. The
78 multi-specimen method can be applied to mixed layers with more than two layer types
79 whatever the layer stacking sequences, and there is no *a priori* limitation to the nature
80 of identified species. It provides also quantitative phase analysis of complex clay
81 parageneses (Drits, 2003).

82 Over the last decade, the multi-specimen method has been widely used to
83 characterize clay mineralogy and its evolution in diagenetic and hydrothermal series
84 (Drits *et al.*, 1997a, 2002a, b, 2004, 2007; Sakharov *et al.*, 1999a, b, 2004; Lindgreen *et*

85 *al.*, 2000, 2002; Claret *et al.*, 2004; McCarty *et al.*, 2004, 2008; Inoue *et al.*, 2005;
86 Aplin *et al.*, 2006; Lanson *et al.*, 2009). Compared with diagenetic and hydrothermal
87 clay parageneses, soil clay species are poorly crystallized and numerous randomly
88 interstratified mixed layers could coexist. To our knowledge, this method has never
89 been applied to soil samples before the present study which investigates the < 2 μ m
90 fraction mineralogy of a Luvisol typical of Western Europe and North America
91 (Jamagne *et al.*, 1984; Velde, 2001). We aimed to demonstrate that, compared with the
92 common identification approach using decomposition and indirect comparison with
93 calculated patterns, profile fitting provides new insights into soil clay mineralogy
94 allowing a more reliable and more complete identification of clay species and the
95 quantification of their relative proportions. This is essential for the understanding of soil
96 genesis and dynamics. A second aim was to investigate whether, the redistribution of
97 clay species between soil horizons and the limited changes of clay crystal structures
98 were consistent with a leaching process.

99

100

101 **Materials and methods**

102 *Soil samples*

103 The studied soil is a “Neo Luvisol” according to the World reference base (IUSS
104 working group WRB, 2006). It is developed on loess deposits from the Closeaux Field
105 Experiment, at the Experimental Station of the Institut National de la Recherche
106 Agronomique (INRA – Château de Versailles, France).

107 On the basis of field observations, five horizons were sampled from the soil profile.
108 Noticeable marks of hydromorphy were observed in the E1g, E2g, Bt and Bt/C
109 horizons, together with accumulation of clays in the pore system of the Bt/C horizon.

110 The relative proportion of the $< 2 \mu\text{m}$ fraction steadily increased with increasing depth
111 from 18% in the surface horizon to 27% in the deeper ones (Table 1). In addition, CEC
112 at the soil pH increased with the increasing content of the $< 2 \mu\text{m}$ fraction from 11.2
113 $\text{cmol}_\text{C} \text{ kg}^{-1}$ in Ap to 16.7 $\text{cmol}_\text{C} \text{ kg}^{-1}$ in Bt/C. The content of organic carbon decreased
114 from 1.6% in the surface horizon to 0.2% in the Bt/C horizon. Finally, the carbonate
115 content was negligible throughout the soil profile, and the cation exchange complex was
116 predominantly saturated with calcium (Ca) (Moni, 2008).

117

118 *Separation of the $< 2 \mu\text{m}$ fraction for X-ray diffraction analysis*

119 No chemical treatments were applied to the raw samples as routine removal of organic
120 matter by using H_2O_2 or of iron and aluminium oxy-hydroxides by using the dithionite-
121 citrate-bicarbonate protocol (Mehra & Jackson, 1960; Moore & Reynolds, 1997) may
122 alter the clay minerals and more especially mixed layer species (Velde *et al.*, 2003).
123 Samples from each soil horizon were first air-dried and sieved to $< 2 \text{ mm}$; 100 g of the
124 sieved sample was then mixed with deionized water and disaggregated by using
125 agitation with glass balls. The $< 50 \mu\text{m}$ fraction was separated next by wet-sieving and
126 dispersed using ultrasonic treatment (20 minutes at 600 W for 400 ml of suspension:
127 Balesdent *et al.*, 1998). The $< 2 \mu\text{m}$ fraction was subsequently isolated from the silt (2-
128 $50 \mu\text{m}$) by using repeated siphoning of the dispersed material (settling for 18 hours at
129 20°C and removal of the upper 22 cm). The extracted suspension was centrifuged, and
130 the remaining supernatant was filtered to $0.45 \mu\text{m}$ and added to the centrifugation
131 ‘residue’, which was then freeze-dried. The clay minerals were studied in their natural
132 state. Consistent with their natural saturation by Ca, a repeated Ca-saturation test (five
133 repeats) did not reveal any difference between natural and Ca-saturated samples (XRD
134 data not shown).

135 Oriented mounts of the $< 2 \mu\text{m}$ fraction were prepared by using the filter transfer
136 method (0.2 μm Nucleopore® polycarbonate filters), as recommended by Moore &
137 Reynolds (1997) for quantitative XRD analysis. Aliquots of 50 mg were deposited on a
138 silicon wafer to avoid scattering from glass. XRD patterns were obtained using a
139 Panalytical X'pert Pro diffractometer equipped with an X'celerator detector ($\text{CuK}\alpha_{1+2}$
140 radiation) in the air-dried state (AD) at room humidity (approximately 35%) and after
141 solvation with liquid ethylene glycol (EG). The size of the divergence, two Soller and
142 antiscatter slits were 0.5° , 2.3° , 2.3° and 0.5° , respectively. Diffraction data were
143 recorded in a scanning mode and converted to step patterns (with a step of $0.017^\circ 2\theta$
144 from 2.5 to $35^\circ 2\theta$, using a 200- second counting time per step).

145 *Decomposition of XRD patterns*

146 Decomposition of AD and EG patterns was performed as recommended by Lanson
147 (1997) over the $3 - 14^\circ 2\theta$ range. Over this angular range, the resolution of the $\text{K}\alpha_{1+2}$
148 doublet is low enough to allow using the Fityk 0.8.2 peak fitting software (Wojdyr,
149 2007). Following background stripping, XRD patterns were fitted with Gaussian
150 elementary curves whose number was steadily increased until a satisfactory fit to the
151 data was obtained. The initial parameters (position and FWHM) of elementary curves
152 were derived from previous studies on similar soil clay parageneses (Righi *et al.*, 1995;
153 Pernes-Debuyser *et al.*, 2003) and optimized with the Levenburg-Marquardt algorithm.
154 When compared, the results obtained were identical to those of DecompXR (data not
155 shown).

156

157 *X-ray profile modelling method*

158 XRD patterns of the five samples were modelled, in both AD and EG states, with the
159 Sybilla© software developed by Chevron™ (Aplin *et al.*, 2006). This program provides

160 a graphic user interface to the algorithm developed initially by Drits & Sakharov (1976)
161 and used recently by Drits *et al.* (1997a) and Sakharov *et al.* (1999a, b). It allows the
162 direct comparison between experimental and calculated XRD profiles, the latter being
163 the sum of all elementary contributions which have been identified.

164 Instrumental and experimental parameters such as horizontal and vertical beam
165 divergence, goniometer radius and slide length were introduced and not further refined.
166 The sigmatar parameter (σ^*) which characterizes the distribution of particle orientation
167 was set for each clay mineral phase as recommended by Rüpung *et al.* (2005). For all
168 layer types z atomic coordinates proposed by Moore & Reynolds (1997) were used after
169 modification to fit the layer thickness values used for simulation; thermal motion
170 parameters (B) were also set as proposed by Moore & Reynolds (1997). The position
171 and amount of interlayer species (H₂O and EG molecules in particular) were considered
172 as variable parameters and varied about the values proposed by Moore & Reynolds
173 (1997) during the fitting process. In bi-hydrated smectite layers (2W), a single plane of
174 H₂O molecules was assumed to be present on each side of the interlayer mid-plane as
175 proposed by Ferrage *et al.* (2005a, b). Illite and smectite structural formulae were
176 similar to those proposed by Laird *et al.* (1991) from the ICP-AES elemental analysis of
177 the < 2 μ m fraction from similar soils (Table 2).

178 For each mixed layer, the number, nature, proportion and stacking sequences of
179 the different layer types were considered as adjustable parameters. In the AD state and
180 under room humidity conditions, expandable layers may be dehydrated (S0w: $d_{001} \sim$
181 1.00 nm), mono-hydrated (S1w: $d_{001} \sim$ 1.25 nm), or bi-hydrated states (S2w: $d_{001} \sim$
182 1.50 nm) (Ferrage *et al.*, 2005b). Illite and S0w layers cannot be differentiated in the
183 AD state, but smectite layers expand following EG solvation to incorporate one or two
184 sheets of EG molecules in their interlayers (S1eg: $d_{001} \sim$ 1.30 nm, and S2eg: $d_{001} \sim$

185 1.68 nm, respectively; Table 2). Finally, the distributions of coherent scattering domain
186 sizes (CSDSs) were assumed to be lognormal and characterized by their mean value
187 (Drits *et al.*, 1997b). The quality of the fit was estimated with the unweighted R
188 parameter (Howard & Preston, 1989) over the $4 - 35^\circ 2\theta$ and the $3.5 - 35^\circ 2\theta$ ranges for
189 AD and EG patterns, respectively, to minimize the influence of the low-angle region
190 where the effect of X-ray scattering becomes significant. The $19 - 22^\circ 2\theta$ and $26.5 -$
191 $27.0^\circ 2\theta$ ranges were excluded for the calculation of R as they contains peaks other than
192 clay $00l$ reflections. For practical reasons, optimization was performed using a trial-and-
193 error approach without automatic refinement of the parameters. To ensure the reliability
194 of the model, both AD and EG patterns of a given sample were fitted with a unique set
195 of structural parameters. The relative proportions of the different clay species in these
196 complex parageneses were also optimized with Sybilla. The multi-specimen approach
197 requires that these proportions to be similar in both AD and EG states.

198

199

200 **Results**

201 *Qualitative description of experimental XRD patterns*

202 XRD patterns obtained on the $< 2 \mu\text{m}$ fraction (AD and EG) of the five soil horizons are
203 shown in Figure 1. All samples contained quartz (0.426 and 0.334 nm peaks), feldspars
204 (0.325 and 0.320 nm) and poorly crystallized goethite (0.418 nm). The clay paragenesis
205 is similar for all horizons including kaolinite (rational series of peaks at 0.716 and
206 0.358 nm in AD and EG states), illite-mica (rational series of peaks at 1.01, 0.498 and
207 0.334 nm in AD and EG states). In addition, the presence of broad and irrational peak
208 series whose position shifts between AD and EG treatments suggests the presence of
209 mixed layers containing expandable layers. Specifically, the 1.47 nm peak observed on

210 the AD pattern shifted to approximately 1.75 nm following EG solvation. Such
211 behaviour is characteristic of randomly interstratified illite-smectite (Moore &
212 Reynolds, 1997). The steady intensity increase of the 1.47 nm peak with increasing
213 depth suggests an increasing proportion of this mixed layer from Ap to Bt horizons.
214 Finally, the presence of a maximum peaking at 0.485 nm, and its behaviour following
215 EG solvation, supports the presence of a mixed layer containing both chlorite and
216 expandable layers.

217

218 *XRD pattern decomposition results*

219 The number of elementary contributions (6 and 7 in AD and EG states, respectively)
220 necessary to fit the data was remarkably similar for all samples, as are their positions,
221 FWHMs, and relative intensities (Figure 2). This overall similarity supports the
222 hypothesis of a constant composition for all clay minerals along the soil profile. The
223 illite-mica peak at approximately 1.00 nm was fitted by using a broad band at 1.020 nm
224 and a sharp one at 1.000 nm, most probably accounting for a broad CSDS distribution.
225 Similarly, the kaolinite peak at 0.716 nm was fitted with broad and sharp maxima
226 peaking at 0.730 and 0.716 nm, respectively. The broad contribution at approximately
227 1.47 nm was fitted also using two elementary contributions. The broad contribution at
228 1.500 nm (1.550 nm for the Bt/C horizon) sharpens, shifted to 1.750 nm and presents an
229 additional peak at 0.930 nm after EG solvation. The sharp peak at 1.460 nm (AD)
230 broadened and shifted to 1.580 nm after EG solvation.

231 In their study of a similar soil, Pernes-Debuyser *et al.* (2003) used NEWMOD to
232 identify the clay minerals present in surface samples. These authors attributed the two
233 bands at 1.450 nm (broad) and 1.540 nm (sharp) to two randomly interstratified illite-
234 smectite having similar contents of illite and S2w layers (50:50) but different CSDS

235 distributions (1-4 and 3-6 layers, respectively). The XRD pattern corresponding to this
236 clay paragenesis was calculated using Sybilla and compared with the data (Figure 3) to
237 assess the validity of the identification proposed by Pernes-Debuyser *et al.* (2003). The
238 profiles of the peaks corresponding to discrete kaolinite and illite were satisfactorily
239 reproduced. The overall profile of the low-angle data, especially that of the EG patterns,
240 was also approximately reproduced. Significant mismatches were, however, observed,
241 especially over the 6 – 11, 14 – 19 and 26 – 35°2 θ ranges, that resulted in an overall
242 poor fit (Figure 3; R = 23.6% and 22.7% for AD and EG states, respectively) and
243 therefore refute the identification proposed by Pernes-Debuyser *et al.* (2003). In
244 particular, the chlorite-expandable mixed layer whose presence was hypothesized from
245 the maximum peaking over the 18 – 19°2 θ range at 0.485 nm (AD) has a probable
246 contribution over the low-angle region.

247

248 *Full pattern fitting*

249 To overcome the limitations of an indirect identification illustrated above, XRD patterns
250 recorded on the oriented clay separates preparations of all horizons were all fitted in
251 both AD and EG states. The optimum fit was obtained systematically with randomly
252 interstratified illite-smectite and chlorite-smectite, in addition to discrete smectite, illite
253 and kaolinite as illustrated for the Bt horizon (Figure 4). The structural characteristics
254 of the optimal models are listed in Tables 2 and 3, and Table 4 contains the relative
255 proportions of the different contributions. Discrete illite contributed to the three
256 reflections at 1.006, 0.499 and 0.333 nm (AD) and 1.001, 0.501 and 0.333 nm (EG).
257 These reflections were sharp, indicative of a large mean CSDS (18 layers – Table 3).
258 Two populations of kaolinite having contrasting CSDS (6 and 20 layers on average)
259 were necessary to fit the low-angle asymmetry of the 0.716 and 0.358 nm reflections. At

260 1.554 nm, the 001 reflection of discrete smectite contributed significantly to the overall
261 intensity of the broad 1.47 nm peak. The 005 reflection (0.305 nm) also accounted for
262 the high-angle tail of the peak at 0.334 nm (AD). Following EG solvation, the first
263 smectite reflection shifted to 1.808 nm accounting for the low-angle asymmetry of the
264 peak at 1.750 nm. The 005 reflection at 0.337 nm contributed to the large ‘background’
265 intensity between the 0.358 and 0.334 nm peaks. Discrete smectite has a small mean
266 CSDS (3 layers) to match the width of experimental maxima. The heterogeneous
267 hydration and swelling behaviours (36:64 S1w:S2w ratio in the AD state, and 24:76
268 S1eg:S2eg ratio after EG salvation: Table 3) also contributes to line broadening. The
269 003 reflection of smectite has a low intensity compared with that of 001 because of the
270 large content of octahedral iron (1.2 atoms by unit formula: Table 2, Laird *et al.*, 1991).

271 A randomly interstratified illite-smectite with a large illite content (63:37
272 illite:smectite ratio) was also identified in the clay paragenesis. This mixed layer has a
273 small CSDS (six layers) and its smectite layers exhibited a heterogeneous hydration and
274 swelling behaviour (Table 3). As a result, its first order reflection (at approximately
275 1.27 nm in the AD state) allowed the high-angle asymmetry of the 1.47 nm peak to be
276 fitted, whereas the 0.503 and 0.322 nm maxima contributed to the low- and high-angle
277 tails of the complex maxima at 0.498 and 0.334 nm, respectively (Figure 4a). Following
278 EG solvation, this randomly interstratified illite-smectite exhibited only weak and
279 poorly-defined modulations over the low-angle region, which make it essentially
280 undetectable using a decomposition approach. This mixed layer thus contributed to the
281 diffracted intensity mostly on the high-angle side of the 0.498 nm peak, and in the
282 complex band at 0.334 nm. A randomly interstratified chlorite-smectite (52:48
283 chlorite:smectite ratio: Table 3) completed the clay paragenesis accounting in particular
284 for the high angle shoulder of the 0.498 nm peak (AD) and for the sharp maximum of

285 the broad 1.47 nm band (Figure 4a). After EG solvation, this mixed layer contributed
286 mostly to the large ‘background’ intensity between the 0.358 and 0.334 nm peaks, and
287 to the complex 1.75 nm band.

288 The same clay paragenesis with discrete kaolinite, illite and smectite, and randomly
289 interstratified illite-smectite and chlorite-smectite was used to fit XRD patterns from all
290 five horizons (Figure 5, Tables 3 and 4) with R factor values ranging from 8.7 – 12.8%
291 and from 9.3 – 12.6% for AD and EG patterns, respectively. The structural
292 characteristics of discrete illite and kaolinite were essentially constant over the entire
293 soil profile. Similarly, discrete smectite was systematically dominated by S2w layers
294 (AD), the relative proportion of which was at a minimum in E1g and E2g horizons at
295 approximately 55%, and increasing to 77% in the Bt/C horizon. Following EG
296 solvation, most smectite layers incorporated two sheets of EG molecules. Consistent
297 with the hydration behaviour, the proportion of S1eg layers was minimal in the E1g
298 horizon (72%) and maximal in Bt/C (94%).

299 The composition of the two mixed layers was also more or less constant along the
300 soil profile with 63% illite in the illite-smectite and 52% chlorite in the chlorite-
301 smectite, except in the most superficial horizon (62% chlorite). In both mixed layers,
302 the hydration behaviour of expandable layers was heterogeneous with 4 – 35% of
303 smectite layers having only one sheet of interlayer H₂O molecules. Following EG
304 solvation, swelling heterogeneity was reduced, especially in the chlorite-smectite (Table
305 3). In the illite-smectite, swelling heterogeneity was more pronounced with 8 – 30% of
306 smectite layers incorporating a single sheet of EG molecules, the proportion of S1eg
307 steadily decreasing with increasing depth.

308 Relative proportions of the various clay species are listed in Table 4. Discrete illite
309 and kaolinite represent approximately 20% of the < 2 µm fraction each, their proportion

310 being constant throughout the profile. The proportion of discrete smectite increased
311 from the Ap (18%) to the Bt horizon (33%) in which it was the dominant clay species.
312 At greater depth in the Bt/C horizon, the proportion of discrete smectite decreased to
313 23%. The randomly interstratified illite-smectite was the dominant clay species
314 throughout the soil profile, except in the Bt horizon, despite its diffuse contribution to
315 the low-angle intensity (Figure 4b). From E2g to Bt horizons, the proportion of this
316 mixed layer decreased from approximately 30 to approximately 25%, increasing again
317 to approximately 30% in the Bt/C horizon. Finally, the chlorite-smectite accounts for 5
318 – 8% of the $< 2 \mu\text{m}$ fraction along the soil profile, without any significant change with
319 depth.

320

321

322 **Discussion**

323 In the present work, pattern fitting led to an innovative interpretation of XRD patterns,
324 providing detailed information on the different phases present in the soil horizons, on
325 their structural evolution and on their relative abundances. In the following discussion
326 the fitting approach will first be compared with numerical tools commonly used for the
327 interpretation XRD patterns (DecompXR, Newmod). The results in terms of
328 pedogenesis will then be discussed.

329

330 *Limitations of the decomposition-XRD calculation approach*

331 The present study allows us to question the combined use of XRD pattern
332 decomposition and indirect identification from elementary peak positions (\pm FWHM) to
333 describe complex clay parageneses commonly encountered in soils, although it has been
334 widely used for this purpose over the last decade (Righi *et al.*, 1995; Righi & Elsass,

335 1996; Velde, 2001; Pernes-Debuyser *et al.*, 2003; Velde *et al.*, 2003; Vingiani *et al.*,
336 2004; Jouquet *et al.*, 2005, 2007; Fontaine *et al.*, 2007; Barré *et al.*, 2007a, b, 2008a, b;
337 Montagne *et al.*, 2008). In particular, the clay mineralogy deduced from such a data
338 processing (illite, kaolinite and two randomly interstratified illite-smectite, Pernes-
339 Debuyser *et al.*, 2003), did not permit the reproduction of XRD data for the samples
340 investigated. Several hypotheses can be proposed to account for this inadequacy.

341 The first is the specific diffraction fingerprint, without any significant peak in the
342 low-angle region, of the randomly interstratified illite-smectite which is the main clay
343 mineral phase in the soil profile. This mixed layer is characterized by a broad and
344 poorly defined contribution to the diffracted intensity. As a consequence, this major
345 contribution is stripped during the initial background removal. This key drawback of the
346 decomposition approach is especially noteworthy for soil clay minerals, as most of them
347 combine small CSDS and complex interstratification, thus giving rise to weakly
348 modulated XRD patterns.

349 The second hypothesis, that indirect identification of mixed layers from their peak
350 position is essentially inadequate, is discussed in detail by Lanson (2005). Specifically,
351 the heterogeneous nature of expandable interlayers hampers the use of simplified peak
352 migration identification techniques based on two-component mixed layers (Drits, 1997;
353 2003). Such hydration/swelling heterogeneity has been found in most natural samples,
354 whatever their origin and mineralogy (Drits *et al.*, 1997a; Sakharov *et al.*, 1999a;
355 Lindgreen *et al.*, 2000; Drits, 2003; McCarty *et al.*, 2004; Inoue *et al.*, 2005; Ferrage *et*
356 *al.*, 2005b, 2007). Again, this drawback is especially important for soils where
357 heterogeneity is expected to be even greater than in other geological settings.

358

359 *New contributions from XRD profile-fitting for interpreting complex clay mineral*
360 *assemblages*

361 The overall agreement, both visually (Figure 5) and quantitatively with R values
362 systematically being < 13%, demonstrates the ability of the multi-specimen approach to
363 provide a good quality fit to experimental data obtained on polyphasic soil samples: this
364 is consistent with previous studies in other geological settings (Drits *et al.*, 1997a,
365 2002a, b, 2004, 2007; Sakharov *et al.*, 1999a, b, 2004; Lindgreen *et al.*, 2000, 2002;
366 Claret *et al.*, 2004; McCarty *et al.*, 2004, 2008; Inoue *et al.*, 2005; Aplin *et al.*, 2006;
367 Lanson *et al.*, 2009). This approach can thus be used to determine accurate structural
368 characteristics for the phases present in a given sample, as well as their relative
369 proportions. The sensitivity of the approach to structural characteristics and phase
370 heterogeneity has been discussed previously (Drits *et al.*, 1997a, 2002b, 2007; Sakharov
371 *et al.*, 1999a; Drits, 2003; Lanson *et al.*, 2009). However, the actual sensitivity of the
372 calculated XRD patterns to key structural characteristics needs to be illustrated. The
373 actual presence of the different contributions is the first of these. In the present work,
374 mixed layers are introduced only if they allowed fitting specific angular ranges without
375 significant overlap with other phases as illustrated in Figure 4. The absence of the small
376 CSDS kaolinite contribution leads, for example, to a significant misfit over the 11 –
377 12°2θ range (Figure 6a). The influence of CSDS is illustrated next. Compared with the
378 optimal fit to the data (Figure 5), increasing the CSDS of discrete smectite from three to
379 five layers leads to evident misfits over the 4 – 6°2θ and 29.5 – 31.5°2θ ranges, whereas
380 decreasing the CSDS of discrete illite from 18 to 13 layers decreased the resolution of
381 the peak at 17.5°2θ (002 reflection: Figure 6b). Finally, sensitivity of calculated profiles
382 to smectite hydration behaviour may be assessed by considering, for example, that all
383 layers are bi-hydrated in discrete smectite. As a result, the 001 reflection was shifted

384 towards smaller angles thus inducing a major misfit over the 4 – 6°2θ range (Figure
385 6c).

386 The next section focuses on the implications of the original description of clay
387 paragenesis obtained from profile fitting for clay pedogenetic processes and more
388 especially for three major issues.

389 Clay paragenesis in Luvisols. From XRD results, Jamagne *et al.* (1984) claim that the
390 clay mineralogy is similar in the different horizons of soils formed on loess deposits,
391 even in the case of intense clay illuviation, and indicate that the < 2 μm fraction
392 includes “kaolinite, mica and a complex group of other layer silicates, including
393 smectite and mixed layers of chloritic, micaceous, vermiculitic and smectitic layers in
394 random interstratification”. Using XRD profile fitting, the present study confirms the
395 interpretation of Jamagne *et al.* (1984) for discrete clay species with the presence of
396 kaolinite, illite and smectite. It also allows an improved description of the “complex
397 group of other silicates” which includes two randomly interstratified illite-smectite
398 (63:37) and chlorite-smectite (52:48). Direct profile fitting thus confirms that in
399 Luvisols the clay paragenesis is stable along the soil profile as proposed by Jamagne *et*
400 *al.* (1984).

401 Structural characteristics of clay species and their development along the profile. Even
402 when looking at a more detailed level, clay mineralogy was remarkably constant along
403 the soil profile. Structural parameters of discrete kaolinite and illite and of illite-smectite
404 and chlorite-smectite phases were similar in the different horizons (Table 3). Some
405 differences were, however, observed at the soil surface. In particular, the chlorite
406 content of the chlorite-smectite increased from 52 to 62% in the topsoil Ap horizon,
407 simultaneously with a decrease of its mean CSDS from nine to seven layers. On the
408 contrary, the mean CSDS of the illite-smectite increases from six to seven layers in the

409 lower horizons to nine layers in the uppermost one (Table 3). The parent material, that
410 is the loess deposit, was thus probably homogeneous. In addition, kaolinite, illite, illite-
411 smectite and chlorite-smectite species did not present significant structural changes
412 along the soil profile compared with discrete smectite. The hydration and swelling
413 (S1w:S2w and S1eg:S2eg ratios, respectively) properties of smectite varied from one
414 horizon to the other, however, without any significant trend with depth. In addition, the
415 relative proportions of S1w and S1eg layers were not strictly correlated, the latter being
416 usually smaller than the former. Except in the Bt/C horizon where smectite was almost
417 fully expanded after EG solvation, the proportion of S1eg layers ranged from 17 to 28%
418 (Table 4). Consistent with our observations, Velde (2001) reported that approximately
419 one third of expandable layers incorporated a single sheet of EG molecules in the
420 surface horizons of cultivated soils, and thus deduced the presence of a similar
421 proportion of high-charge expandable layers. However, in our case the heterogeneous
422 swelling observed for discrete smectite is possibly induced by sample preparation
423 artefacts. No sample pre-treatments were performed to remove organic matter and iron
424 oxy-hydroxides prior to size fractionation. Such pre-treatments were performed on
425 sample aliquots to extract the $< 0.05 \mu\text{m}$ size fraction. These fractions, which
426 concentrate discrete smectite, were X-rayed following solvation by EG vapour
427 (16 hours at 40°C under vacuum). The results obtained (not shown) showed no
428 difference between Ap and Bt horizons with 100% of S2eg layers in both cases. The
429 intimate mixing of organic matter and/or of iron oxy-hydroxides with clays is thus
430 likely to be responsible for the observed reduced expandability of smectite, and for the
431 observed variation of smectite swelling behaviour along the profile.

432 Quantitative phase analysis. Direct profile fitting method overcomes the intrinsic
433 limitations of the decomposition approach, which was restricted to peak intensity ratios

434 between similar clay species, and provides reliable estimates of the phase composition
435 for complex clay parageneses (Drits *et al.*, 1997a; Lindgreen *et al.*, 2002; Claret *et al.*,
436 2004; McCarty *et al.*, 2008; Lanson *et al.*, 2009). Jamagne *et al.* (1984) concluded that
437 the relative contents of mica and trioctahedral chlorite increase close to the soil surface
438 as the result of the physical breakdown of coarse particles and/or of the preferential
439 migration of other minerals as reported also in Belgian soils (Van Ranst *et al.*, 1982). In
440 our work, we show that the relative proportion of discrete smectite increases from 18%
441 (Ap horizon), to approximately 25% (E1g and E2g horizons), and to 33% (Bt horizon –
442 Table 4). This proportion decreases to 25% in the Bt/C horizon. The contribution of
443 discrete smectite increases essentially at the expense of illite-smectite, which dominated
444 the clay paragenesis in all horizons but B. Discrete kaolinite and illite and chlorite-
445 smectite were also affected but to a lesser extent because of their smaller abundances. In
446 addition, the increase in the < 2 µm fraction content with increasing depth may further
447 attenuate the impact on these clay species. The present results are thus consistent with
448 the leaching process described for Luvisols, and more especially with undisturbed
449 column leaching experiments performed with the same soil (Rousseau *et al.*, 2004).

450

451

452 **Conclusions**

453 The present study demonstrates that the combined use of XRD pattern decomposition
454 and indirect identification from peak positions does not allow a complete identification
455 of complex clay parageneses such as those commonly encountered in soils. However,
456 when carefully used (see recommendations of Lanson, 1997), this approach can be a
457 relevant preliminary step in the study of clay mineral evolution in soils formed on
458 homogenous parent materials.

459 A complete, accurate and quantitative mineralogical characterization of complex
460 clay parageneses requires fitting the data with a pattern calculated for a hypothesized
461 mineral assemblage. Additional constraints can be obtained for a given sample by fitting
462 various XRD patterns obtained after different treatments. Using this multi-specimen
463 approach, structural characteristics and relative proportions of both discrete and mixed
464 layer clays are obtained. The present study demonstrates that, although time-consuming,
465 the multi-specimen approach can be applied to soil samples. The resulting mineralogical
466 characterization of clays can then serve as the basis for studying their individual
467 structural evolution, and that of their relative abundances along the profile.

468 In particular, it is shown in the present Luvisol profile that the structural
469 characteristics of all clay minerals are essentially constant over the entire profile, thus
470 reflecting the mineralogy of the parent material. As reported in the literature
471 (Duchaufour & Lelong, 1967; Jamagne, 1973; Pedro *et al.*, 1978; Jamagne *et al.*, 1984),
472 pedogenesis ongoing in Luvisols affects, essentially, the vertical distribution of the
473 different clay species as the result of particle migration. Our results indicate that the
474 relative increase of smectite has a major contribution to the overall increase of the
475 $< 2 \mu\text{m}$ fraction with increasing depth. This interpretation of the mineralogical data is in
476 agreement with the leaching process described for Luvisols in the literature and may be
477 valid for other soils formed on loess deposits which are common in North America and
478 Western Europe and used to grow crops. As the proposed approach allows us to gain
479 detailed information on the structural evolution of individual clay species, further
480 research could aim at determining the impact of fertilizers, human activities or plant
481 nutrient uptake on the development of soil minerals. In addition, the complete and
482 quantitative mineralogical characterization allows the comparison of clay parageneses
483 in soils derived from different parent materials.

484

485

486 **Acknowledgments**

487 Financial support from the ANR ECCO PCBB ‘Carbone profond’ (ANR-05-ECCO-
488 011-04) program and HydrASA is acknowledged. The authors are grateful to Chevron
489 Energy Technology Company, a division of Chevron U.S.A. Inc., which freely allowed
490 using the Sybilla[®] software for academic purposes. The authors are especially indebted
491 to Dr. Doug McCarty for its sustained help with Sybilla[®]. Dr. C. Moni and Professor C.
492 Chenu (BioEMCO, France) kindly provided the soil samples.

493 **References**

- 494 Aplin, A.C., Matenaar, I.F., McCarty, D.K. & van der Pluijm, B.A. 2006. Influence of
495 mechanical compaction and clay mineral diagenesis on the microfabric and pore-
496 scale properties of deep-water Gulf of Mexico mudstones. *Clays & Clay Minerals*,
497 **54**, 500-514.
- 498 Balesdent, J., Besnard, E., Arrouays, D. & Chenu, C. 1998. The dynamics of carbon in
499 particle-size fractions of soil in a forest-cultivation sequence. *Plant & Soil*, **201**, 49-
500 57.
- 501 Barré, P., Velde, B. & Abbadie, L. 2007a. Dynamic role of "illite-like" clay minerals in
502 temperate soils: Facts and hypotheses. *Biogeochemistry*, **82**, 77-88.
- 503 Barré, P., Velde, B., Catel, N. & Abbadie, L. 2007b. Soil-plant potassium transfer:
504 Impact of plant activity on clay minerals as seen from X-ray diffraction. *Plant &*
505 *Soil*, **292**, 137-146.
- 506 Barré, P., Montagnier, C., Chenu, C., Abbadie, L. & Velde, B. 2008a. Clay minerals as
507 a soil potassium reservoir: observation and quantification through X-ray diffraction.
508 *Plant & Soil*, **302**, 213-220.
- 509 Barré, P., Velde, B., Fontaine, C., Catel, N. & Abbadie, L. 2008b. Which 2:1 clay
510 minerals are involved in the soil potassium reservoir? Insights from potassium
511 addition or removal experiments on three temperate grassland soil clay assemblages.
512 *Geoderma*, **146**, 216-223.
- 513 Claret, F., Sakharov, B.A., Drits, V.A., Velde, B., Meunier, A., Griffault, L. & Lanson,
514 B. 2004. Clay minerals in the Meuse-Heute Marne underground laboratory (France):
515 Possible influence of organic matter on clay mineral evolution. *Clays & Clay*
516 *Minerals*, **52**, 515–532.

- 517 Dixon, J.B. & Weed, S.B. 1989. *Minerals in Soil Environments*. Soil Science Society of
518 America Inc., Madison.
- 519 Drits, V.A. 1997. Mixed-layer minerals. In: *EMU Notes in Mineralogy, Volume 1* (ed.
520 S. Merlino), pp. 153-190. Eötvös University Press, Budapest.
- 521 Drits, V.A. 2003. Structural and chemical heterogeneity of layer silicates and clay
522 minerals. *Clay Minerals*, **38**, 403-432.
- 523 Drits, V.A. & Sakharov, B.A. 1976. *X-ray Structural Analysis of Mixed-layer Minerals*.
524 Nauka, Moscow. (In Russian).
- 525 Drits, V.A. & Tchoubar C. 1990. *X-ray diffraction by disordered lamellar structures:
526 Theory and applications to microdivided silicates and carbons*. Springer-Verlag,
527 Berlin.
- 528 Drits, V.A., Lindgreen, H., Sakharov, B.A. & Salyn, A.L. 1997a. Sequential structure
529 transformation of illite-smectite-vermiculite during diagenesis of Upper Jurassic
530 shales, North Sea. *Clay Minerals*, **33**, 351-371.
- 531 Drits, V.A., Srodon, J. & Eberl, D.D. 1997b. XRD measurement of mean crystallite
532 thickness of illite and illite/smectite: reappraisal of the kubler index and the scherrer
533 equation. *Clays & Clay Minerals*, **45**, 461-475.
- 534 Drits, V.A., Lindgreen, H., Sakharov, B.A., Jakobsen, H.J., Salyn, A.L. & Dainyak,
535 L.G. 2002a. Tobelitization of smectite during oil generation in oil-source shales.
536 Application to North Sea illite-tobelite-smectite-vermiculite. *Clays & Clay Minerals*,
537 **50**, 82-98.
- 538 Drits, V.A., Sakharov, B.A., Dainyak, L.G., Salyn, A.L. & Lindgreen, H. 2002b.
539 Structural and chemical heterogeneity of illite-smectites from Upper Jurassic

540 mudstones of East Greenland related to volcanic and weathered parent rocks.
541 *American Mineralogist*, **87**, 1590-1607.

542 Drits, V.A., Lindgreen, H., Sakharov, B.A., Jacobsen, H.J. & Zviagina, B.B. 2004. The
543 detailed structure and origin of clay minerals at the Cretaceous/Tertiary boundary,
544 Stevns Klint (Denmark). *Clay Minerals*, **39**, 367-390.

545 Drits, V.A., Lindgreen, H., Sakharov, B.A., Jakobsen, H.J., Fallick, A.E., Salyn, A.L.,
546 Dainyak, L.G., Zviagina, B.B. & Barfod, D.N. 2007. Formation and transformation
547 of mixed-layer minerals by Tertiary intrusives in Cretaceous mudstones, West
548 Greenland. *Clays & Clay Minerals*, **55**, 260-283.

549 Duchaufour, P. & Lelong, F. 1967. Entraînement et destruction d'argile dans les
550 horizons éluviaux des sols lessivés. *Comptes Rendus de l'Académie des Sciences*
551 *série D*, **264**, 2884-2887.

552 Egli, M., Mirabella, A. & Fitze, P. 2001. Clay mineral formation in soils of two
553 different chronosequences in the Swiss Alps. *Geoderma*, **104**, 145-175.

554 Egli, M., Nater, M., Mirabella, A., Raimondi, S., Plötze, M. & Alioth, L. 2008. Clay
555 minerals, oxyhydroxide formation, element leaching and humus development in
556 volcanic soils. *Geoderma*, **143**, 101-114.

557 Ferrage, E., Lanson, B., Malikova, N., Plançon, A., Sakharov, B.A. & Drits, V.A.
558 2005a. New insights on the distribution of interlayer water in bi-hydrated smectite
559 from X-ray diffraction profile modeling of 00l reflections. *Chemistry of Materials*,
560 **17**, 3499-3512.

561 Ferrage, E., Lanson, B., Sakharov, B.A. & Drits, V.A. 2005b. Investigation of smectite
562 hydration properties by modeling of X-ray diffraction profiles. Part 1.
563 Montmorillonite hydration properties. *American Mineralogist*, **90**, 1358-1374.

- 564 Ferrage, E., Lanson, B., Sakharov, B.A., Geoffroy, N., Jacquot, E. & Drits, V.A. 2007.
565 Investigation of dioctahedral smectite hydration properties by modeling of X-ray
566 diffraction profiles: Influence of layer charge and charge location. *American*
567 *Mineralogist*, **92**, 1731-1743.
- 568 Fontaine, S., Barot, S., Barré, P., Bdioui, N., Mary, B. & Rumpel, C. 2007. Stability of
569 organic carbon in deep soil layers controlled by fresh carbon supply. *Nature*, **450**,
570 277-280.
- 571 Hardy, M., Jamagne, M., Elsass, F., Robert, M. & Chesneau, D. 1999. Mineralogical
572 development of the silt fractions of a Podzoluvisol on loess in the Paris Basin
573 (France). *European Journal of Soil Science*, **50**, 443-456.
- 574 Howard, S.A. & Preston, K.D. 1989. Profile fitting of powder diffraction patterns. In:
575 *Modern Powder Diffraction* (eds D.L. Bish & J.E.Post), pp. 217-275. Mineralogical
576 Society of America, Chantilly.
- 577 Inoue, A. *et al.* 2005. Illite-smectite mixed-layer minerals in the hydrothermal alteration
578 of volcanic rocks: I. One-dimensional XRD structure analysis and characterization of
579 component layers. *Clays & Clay Minerals*, **53**, 423-439.
- 580 IUSS working group WRB. 2006. *World Reference Base for Soil Resources*. World Soil
581 Resources Reports N° 103. FAO, Rome.
- 582 Jamagne, M. 1973. *Contribution à l'étude pédogénétique des formations loessiques du*
583 *Nord de la France*. Ph.D. thesis, Faculté des Sciences Agronomiques, Gembloux.
- 584 Jamagne, M., De Coninck, F., Robert, M. & Maucorps, J. 1984. Mineralogy of clay
585 fractions of some soils on loess in northern France. *Geoderma*, **33**, 319-342.

- 586 Jouquet, P., Barré, P., Lepage, M. & Velde, B. 2005. Impact of subterranean fungus-
587 growing termites (Isoptera, Macrotermitiae) on chosen soil properties in a West
588 African savanna. *Biology & Fertility of Soils*, **41**, 365-370.
- 589 Jouquet, P., Bottinelli, N., Lata, J.C., Mora, P. & Caquineau, S. 2007. Role of the
590 fungus-growing termite *Pseudacanthotermes spiniger* (Isoptera, Macrotermitinae) in
591 the dynamic of clay and soil organic matter content. An experimental analysis.
592 *Geoderma*, **139**, 127-133.
- 593 Laird, D.A., Barak, P., Nater, E.A. & Dowdy, R.H. 1991. Chemistry of smectitic and
594 illitic phases in interstratified soil smectite. *Soil Science Society of America Journal*,
595 **55**, 1499-1504.
- 596 Lanson, B. 1997. Decomposition of experimental X-ray diffraction profile (profile
597 fitting): A convenient way to study clay minerals. *Clays & Clay Minerals*, **45**, 132-
598 146.
- 599 Lanson, B. 2005. Crystal structure of mixed-layer minerals and their X-ray
600 identification: New insights from X-ray diffraction profile modeling. *Clay Science*,
601 **12** (suppl. 1), 1-5.
- 602 Lanson, B. & Besson, G. 1992. Characterisation of the end of smectite-to-illite
603 transformation: Decomposition of x-ray patterns. *Clays & Clay Minerals*, **40**, 40-52.
- 604 Lanson, B., Sakharov, B.A., Claret, F. & Drits, V.A. 2009. Diagenetic smectite-to-illite
605 transition in clay-rich sediments: A reappraisal of X-ray diffraction results using the
606 multi-specimen method. *American Journal of Science*, **309**, 476-516.
- 607 Lindgreen, H., Drits, V.A., Sakharov, B.A., Salyn, A.L., Wrang, P. & Dainyak, L.G.
608 2000. Illite-smectite structural changes during metamorphism in black Cambrian
609 Alum shales from the Baltic area. *American Mineralogist*, **85**, 1223-1238.

610 Lindgreen, H., Drits, V.A., Sakharov, B.A., Jakobsen, H.J., Salyn, A.L., Dainyak, L.G.
611 & Krøyer, H. 2002. The structure and diagenetic transformation of illite-smectite and
612 chlorite-smectite from North Sea Cretaceous-Tertiary chalk. *Clay Minerals*, **37**, 429-
613 450.

614 McCarty, D.K., Drits, V.A., Sakharov, B., Zviagina, B.B., Ruffell, A. & Wach, G. 2004.
615 Heterogeneous mixed-layer clays from the Cretaceous, Greensand, Isle of Wight,
616 southern England. *Clays & Clay Minerals*, **52**, 552-575.

617 McCarty, D.K., Sakharov, B.A. & Drits, V.A. 2008. Early clay diagenesis in gulf coast
618 sediments: new insights from XRD profile modeling. *Clays & Clay Minerals*, **56**,
619 359-379.

620 Mehra, O.P. & Jackson, M.L. 1960. Iron oxide removal from soils and clay by
621 dithionite-citrate system buffered with sodium bicarbonate. *Clays & Clay Minerals*,
622 **7**, 317-327.

623 Moni, C. 2008. *Stabilisation physique et physico-chimique de la matière organique*
624 *dans les horizons profonds du sol*. Ph.D. thesis, Université Pierre et Marie Curie,
625 Paris 6.

626 Montagne, D., Cornu, S., Le Forestier, L., Hardy, M., Josière, O., Caner, L. & Cousin, I.
627 2008. Impact of drainage on soil-forming mechanisms in a French Albeluvisol: Input
628 of mineralogical data in mass-balance modelling. *Geoderma*, **145**, 426-438.

629 Moore, D.M. & Reynolds, R.C., Jr. 1997. *X-Ray Diffraction and the Identification and*
630 *Analysis of Clay Minerals*. . Oxford University Press, Oxford.

631 Pedro, G., Jamagne, M. & Begon, J.C. 1978. Two routes in genesis of strongly
632 differentiated acid soils under humid, cool-temperate conditions. *Geoderma*, **20**, 173-
633 189.

- 634 Pernes-Debuyser, A., Pernes, M., Velde, B. & Tessier, D. 2003. Soil mineralogy
635 evolution in the INRA 42 plots experiment (Versailles, France). *Clays & Clay*
636 *Minerals*, **51**, 577-584.
- 637 Reynolds, R.C., Jr. 1985. *NEWMOD: A Computer Program for the Calculation of One-*
638 *dimensional Patterns of Mixed-layered Clays*. Reynolds, R.C., Jr, Hanover.
- 639 Righi, D. & Elsass, F. 1996. Characterization of soil clay minerals: decomposition of X-
640 ray diffraction diagrams and high-resolution electron microscopy. *Clays & Clay*
641 *Minerals*, **44**, 791-800.
- 642 Righi, D. & Meunier, A. 1991. Characterization and genetic interpretation of clays in an
643 acid brown soil (Dystrochrept) developed in a granitic saprolite. *Clays & Clay*
644 *Minerals*, **39**, 519-530.
- 645 Righi, D., Velde, B. & Meunier, A. 1995. Clay stability in clay-dominated soil systems.
646 *Clay Minerals*, **30**, 45-54.
- 647 Rousseau, M., Di Pietro, L., Angulo-Jaramillo, R., Tessier, D. & Cabibel, B. 2004.
648 Preferential Transport of Soil Colloidal Particles: Physicochemical Effects on
649 Particle Mobilization. *Vadose Zone Journal*, **3**, 247-261.
- 650 Rüping, K., Dohrmann, R., Jahn, R. & Kleber, M. 2005. Texturmessungen an
651 Tonmineralen in orientierten Präparaten - Eine kritische Diskussion zur
652 Tonmineralquantifizierung. In: *DTTG 2005* (eds R. Dohrmann. & S. Kaufhold.), pp.
653 56-72. Deutsche Ton-und Tonmineralgruppe e.V., Celle.
- 654 Sakharov, B.A., Lindgreen, H., Salyn, A.L. & Drits, V.A. 1999a. Determination of
655 illite-smectite structures using multispecimen XRD profile fitting. *Clays & Clays*
656 *Minerals*, **47**, 555-566.

- 657 Sakharov, B.A., Lindgreen, H. & Drits, V.A. 1999b. Mixed-layer kaolinite-illite-
658 vermiculite in North Sea shales. *Clay Minerals*, **34**, 333-344.
- 659 Sakharov, B.A., Dubinska, E., Bylina, P., Kozubowski, J.A., Kapro, G. & Frontczak-
660 Baniewicz, M. 2004. Serpentine-smectite interstratified minerals from Lower Silesia
661 (SW Poland). *Clays & Clay Minerals*, **52**, 55-65.
- 662 Van Ranst, E., De Coninck, F., Tavernier, R. & Langohr, R. 1982. Mineralogy in silty
663 to loamy soils of central and high Belgium in respect to autochthonous and
664 allochthonous materials. *Bulletin de la Société Belge de Géologie*, **91**, 27-44.
- 665 Velde, B. 2001. Clay minerals in the agricultural surface soils in the Central United
666 States. *Clay Minerals*, **36**, 277-294.
- 667 Velde, B., Goffé, B. & Hoellard, A. 2003. Evolution of clay minerals in a
668 chronosequence of poldered sediments under the influence of a natural pasture
669 development. *Clays & Clay Minerals*, **51**, 205-217.
- 670 Vingiani, S., Righi, D., Petit, S. & Terribile, F. 2004. Mixed-layer kaolinite-smectite
671 minerals in a red-black soil sequence from basalt in Sardinia (Italy). *Clays & Clay
672 Minerals*, **52**, 473-483.
- 673 Wilson, M.J. 1999. The origin and formation of clay minerals in soils: Past, present and
674 future perspectives. *Clay Minerals*, **34**, 7-25.
- 675 Wojdyr, M. 2007. *Fityk 0.8.2 free software*. Wojdyr, M. (At:
676 <http://www.unipress.waw.pl/fityk>. Accessed: 12/05/2009).

677 **FIGURE CAPTIONS**

678

679 **Figure 1.** Experimental XRD patterns obtained for the $< 2 \mu\text{m}$ fraction of the five soil
680 horizons. Black and gray solid lines represent XRD patterns recorded in AD and EG
681 states, respectively. Dashed lines indicate the positions of the main reflections (peak
682 positions in nm).

683 **Figure 2.** Decomposition of XRD data. The experimental XRD patterns and the best fit
684 are shown as grey crosses and as solid lines, respectively. Elementary Gaussian
685 contributions are shown as solid grey lines.

686 **Figure 3.** Comparison between experimental (grey crosses) and calculated (solid lines)
687 XRD patterns for the Ap horizon. (a) AD pattern; (b) EG pattern. The calculated pattern
688 corresponds to the clay paragenesis determined by Pernes-Debuyser et al., (2003) for a
689 similar Ap horizon. The broken x-axis indicates a modified scale factor ($\times 3.5$) for the
690 high-angle region. The grey boxes correspond to angular ranges excluded for the
691 calculation of the quality-of-fit estimate (R parameter). 679

692 **Figure 4.** Elementary contributions to the diffracted intensity for the Bt horizon.
693 Patterns as for Figure 3. The broken x-axis indicates a modified scale factor ($\times 3.0$) for
694 the high-angle region. (a) AD pattern; (b) EG pattern. The positions of the main maxima
695 are given in nm. The kaolinite contribution includes the two sub-populations having
696 different CSDS. The structural parameters for the optimal models are given in Tables 2
697 and 3, the relative proportions of the different contributions in Table 4.

698 **Figure 5.** Comparison between experimental XRD patterns (grey crosses) and
699 optimum multi-specimen fits (solid line) for the 5 horizons (Ap, E1g, E2g, Bt and Bt/C)
700 of the Luvisol. (a) Air-dried and (b) EG solvated samples. Difference plots are shown at

701 the bottom of the Figure. The structural parameters used for these fits are provided in
702 Tables 2 and 3, the relative proportions of the different contributions in Table 4.

703 **Figure 6.** Sensitivity of calculated XRD patterns to the mineralogical composition and
704 structural characteristics. Arrows indicate significant misfits compared with the
705 optimum fit shown in Figure 5a (Bt horizon). The optimum structural characteristics
706 and mineralogical composition are given in Tables 3 and 4, respectively. (a) XRD
707 pattern calculated without the contribution of kaolinite having low CSDS. (b) CSDS of
708 discrete smectite are increased from three (optimum) to five layers whereas that of
709 discrete illite is decreased from 17 (optimum) to 13 layers. (c) All layers are considered
710 to be bi-hydrated in discrete smectite.

1 **Table 1** Main chemical and physical features of the soil profile studied (adapted from Moni, 2008)

Horizon	Depth /cm	Particle size fraction / μm			OC	CaCO ₃ eq. /g kg ⁻¹	pH	CECe	Exchangeable cations			
		0-2	2-50	50-2000					Ca ⁺⁺	Mg ⁺⁺	Na ⁺	K ⁺
Ap	0-30	18	57	25	16.10	< 1	6.5	11.2	9.73	0.90	0.03	0.57
E1g	30-45	19	61	20	6.36	1.8	7.2	12.1	11.50	0.86	0.04	0.18
E2g	45-80	21	50	29	3.95	< 1	7.5	12.8	11.27	0.92	0.04	0.18
Bt	80-100	24	47	29	3.38	1.1	7.7	14.6	11.50	1.35	0.05	0.20
Bt/C	100-135	27	48	25	1.80	< 1	7.9	16.7	12.03	1.81	0.08	0.27

2 OC: organic carbon

3 CaCO₃ eq.: calcium carbonate equivalent

4 CECe: cation exchange capacity at soil pH

1 **Table 2** Structural parameters of the different clay layers.

layer type	Layer thickness /nm	Interlayer cation content ^a	Octahedral iron content ^a
discrete illite	1.000	1.5	0.0
illite in mixed layers	1.000	1.0	0.5
smectite (S1w) ^b	1.250	0.5	1.2
smectite (S2w) ^b	1.500	0.5	1.2
smectite (S1eg) ^b	1.300	0.5	1.2
smectite (S2eg) ^b	1.680	0.5	1.2
chlorite	1.420	-	0.0
kaolinite	0.716	-	-

2 ^a number of atoms per formula unit

3 ^b S1w: smectite with 1 sheet of interlayer H₂O molecules; S2w: smectite with 2 sheets

4 of interlayer H₂O molecules; S1eg: smectite with 1 sheet of interlayer EG molecules;

5 S2eg: smectite with 2 sheets of interlayer EG molecules

1 **Table 3** Composition and structural parameters of clay minerals in the different soil
 2 horizons

Phases	Horizon	Ap	E1g	E2g	Bt	Bt/C
illite	σ^*	17	17	17	17	17
	CSDS	18	18	18	18	18
	I/S2w ^a	98/2	97/3	97/3	95/5	97/3
	I/S2eg ^a	98/2	97/3	97/3	97/3	97/3
kaolinite	σ^*	18	18	18	18	18
	CSDS	20	20	20	20	20
kaolinite	σ^*	18	18	18	18	18
	CSDS	6	6	6	6	6
smectite	σ^*	21	21	21	21	21
	CSDS	3	3	3	3	3
	S1w/S2w ^a	33/67	46/54	47/53	36/64	23/77
	S1eg/S2eg ^a	21/79	28/72	17/83	24/76	6/94
illite-smectite (R0)	σ^*	17	17	17	17	17
	CSDS	9	6	6	6	7
	I/S1w/S2w ^a	63/6/31	63/13/24	63/11/26	63/13/24	63/7/30
	I/S1eg/S2eg ^a	57/13/30	63/7/30	63/3/34	63/8/29	63/3/34
chlorite-smectite (R0)	σ^*	17	17	17	17	17
	CSDS	7	9	9	9	9
	Ch/S1w/S2w ^a	62/13/25	52/11/37	52/6/42	52/2/46	52/8/40
	Ch/S1eg/S2eg ^a	62/0/38	52/0/48	52/6/42	52/0/48	52/0/48

3 σ^* : Parameter characterizing the orientation of particles on the X-ray slide

4 CSDS: Coherent scattering domain size expressed in layers

5 ^a S1w: smectite with 1 sheet of interlayer H₂O molecules; S2w: smectite with 2 sheets

6 of interlayer H₂O molecules; S1eg: smectite with 1 sheet of interlayer EG molecules;

7 S2eg: smectite with 2 sheets of interlayer EG molecules; I: illite layers both in discrete

8 illite and in mixed layers

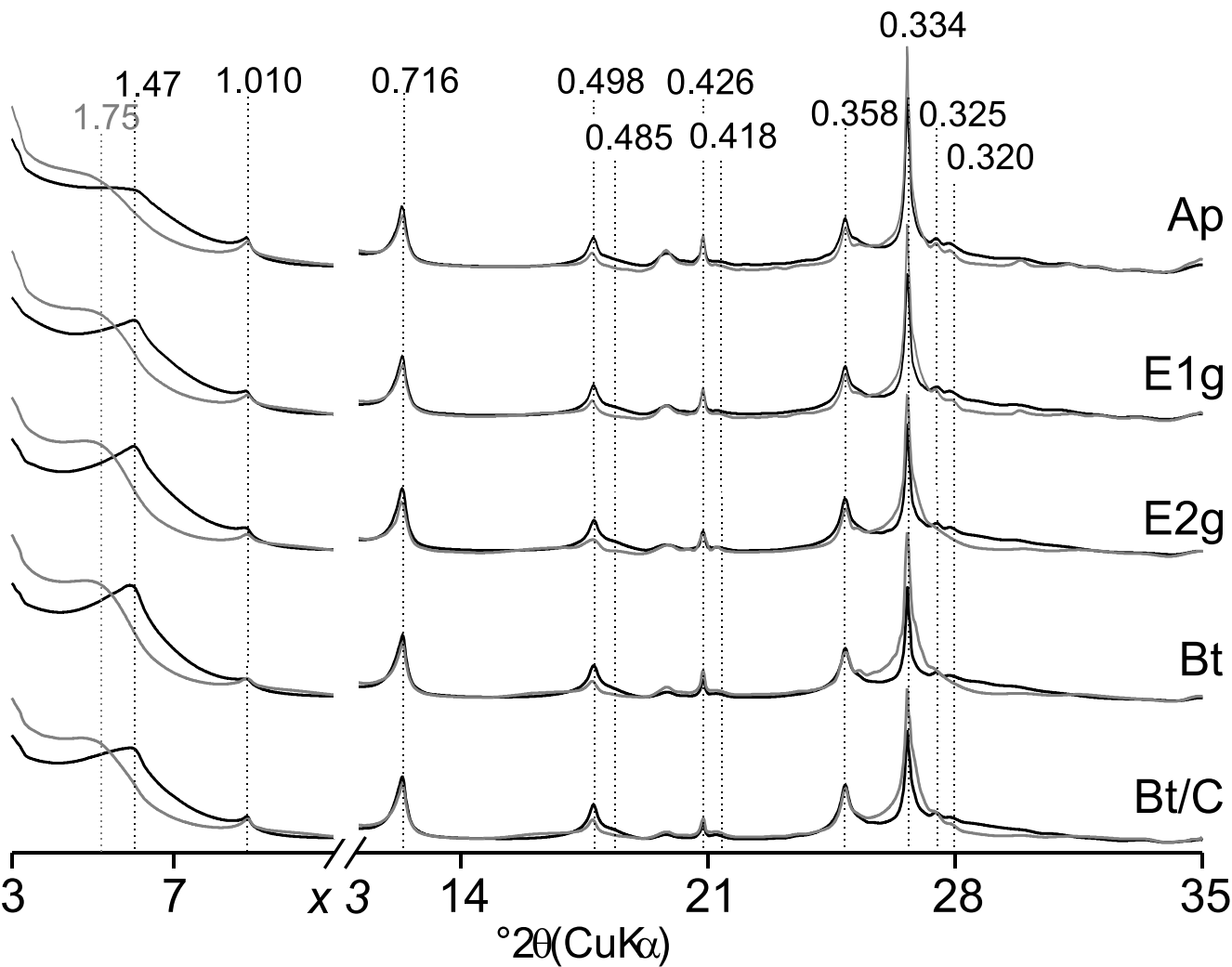
1 **Table 4** Relative proportions (in weight percent) of the different contributions to the
 2 diffracted intensity

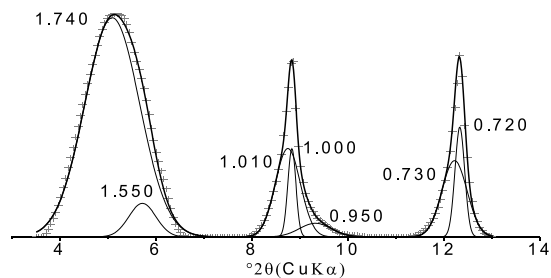
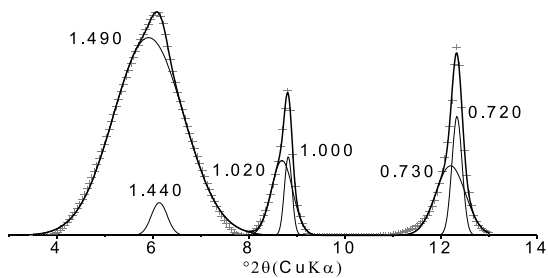
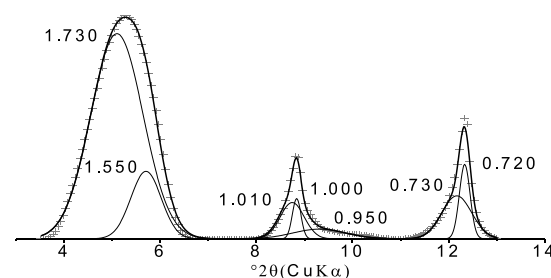
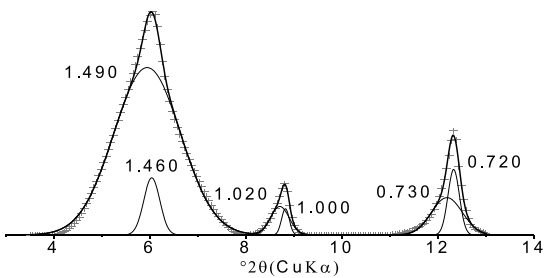
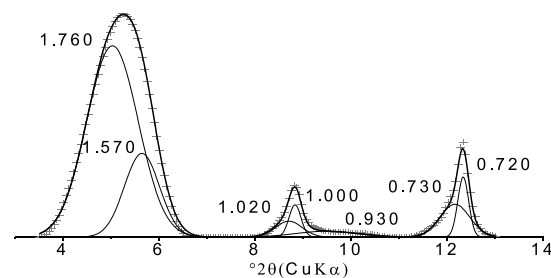
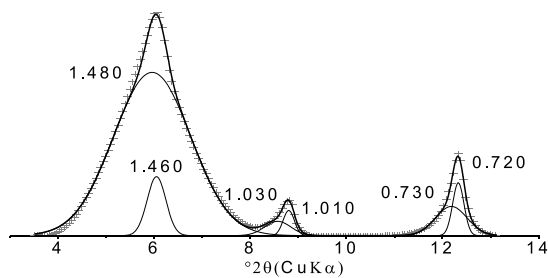
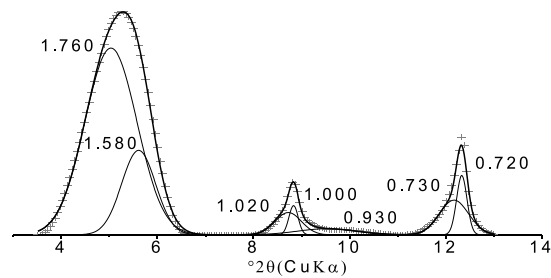
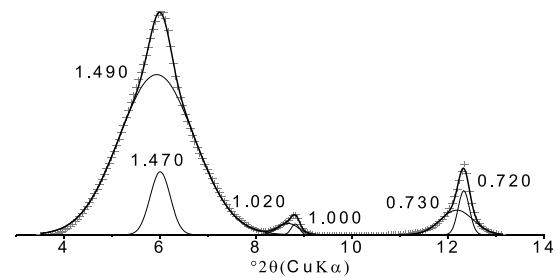
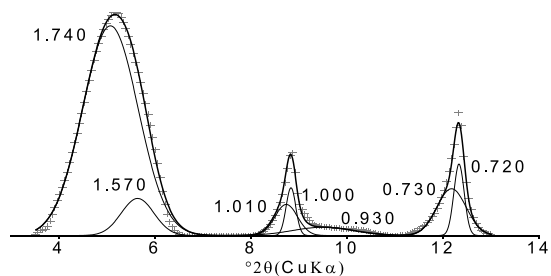
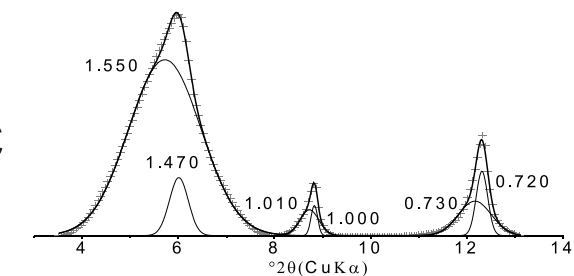
Sample		illite	kaolinite (high CSDS)	kaolinite (low CSDS)	smectite	illite- smectite	chlorite- smectite
Ap	AD	20	12	9	18	33	8
	EG	18	9	10	18	38	7
E1g	AD	22	11	9	24	28	6
	EG	21	9	9	27	29	5
E2g	AD	18	11	9	25	31	6
	EG	17	11	8	26	33	5
Bt	AD	18	11	7	33	24	6
	EG	17	10	7	32	26	8
Bt/C	AD	21	12	8	23	30	6
	EG	18	11	9	23	32	7

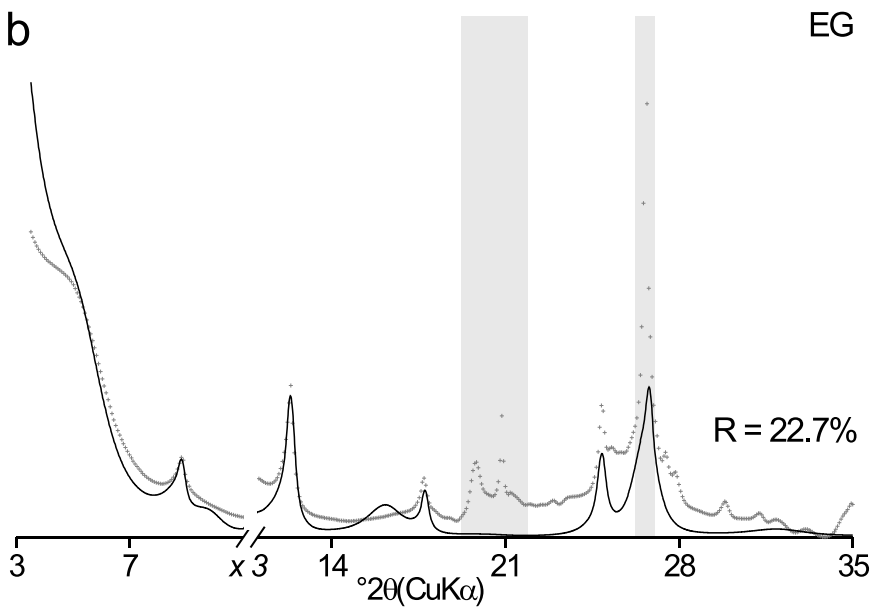
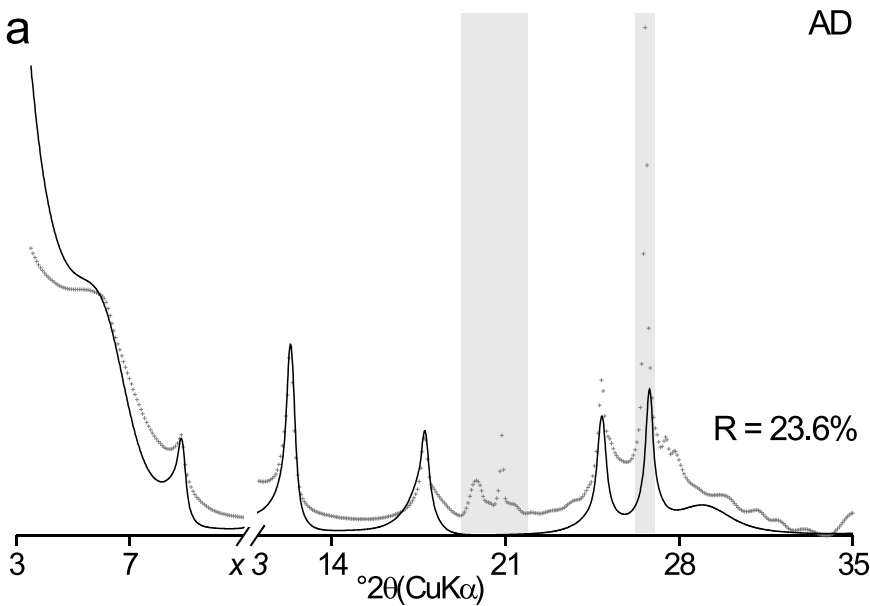
3 CSDS: Coherent scattering domain size

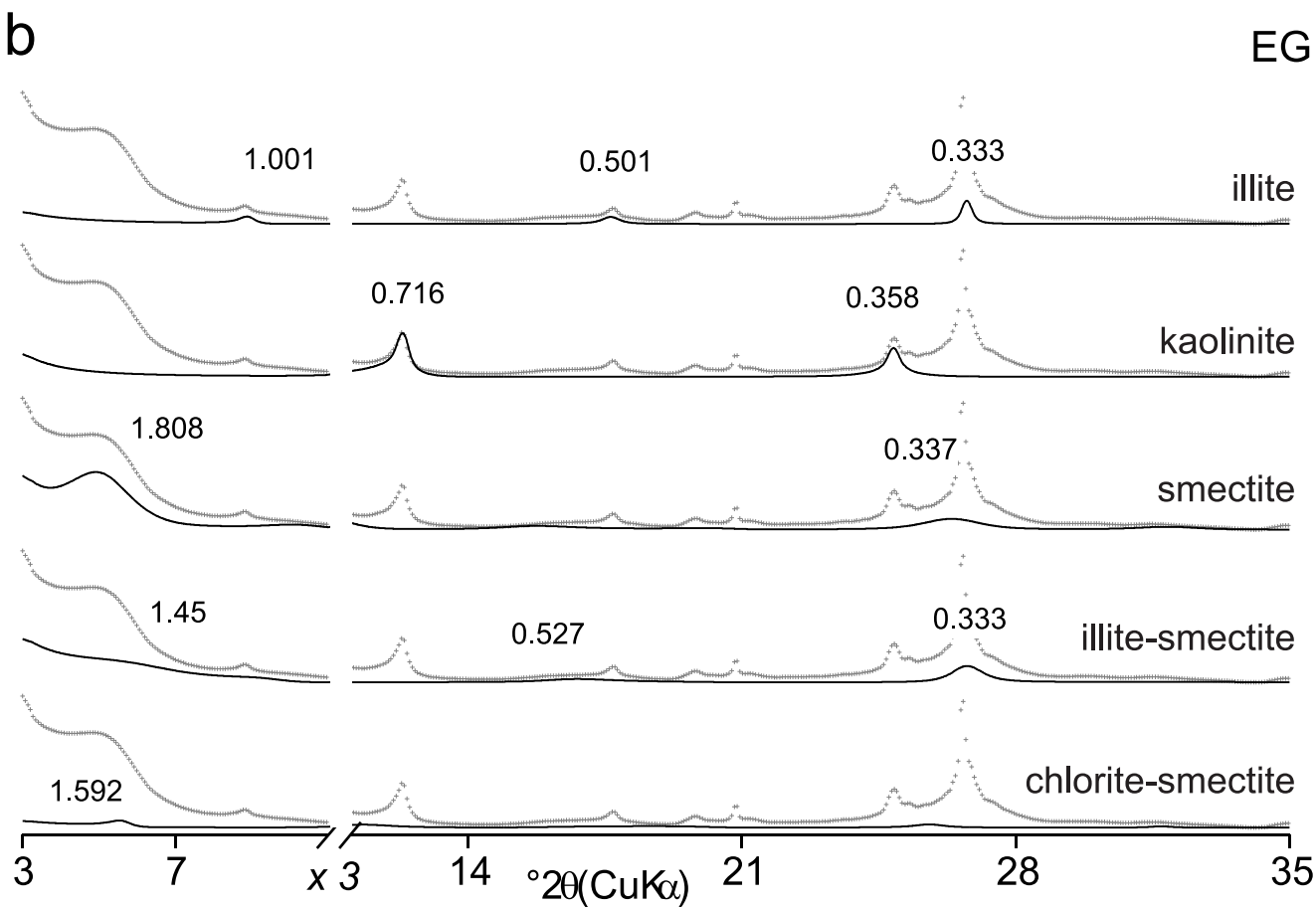
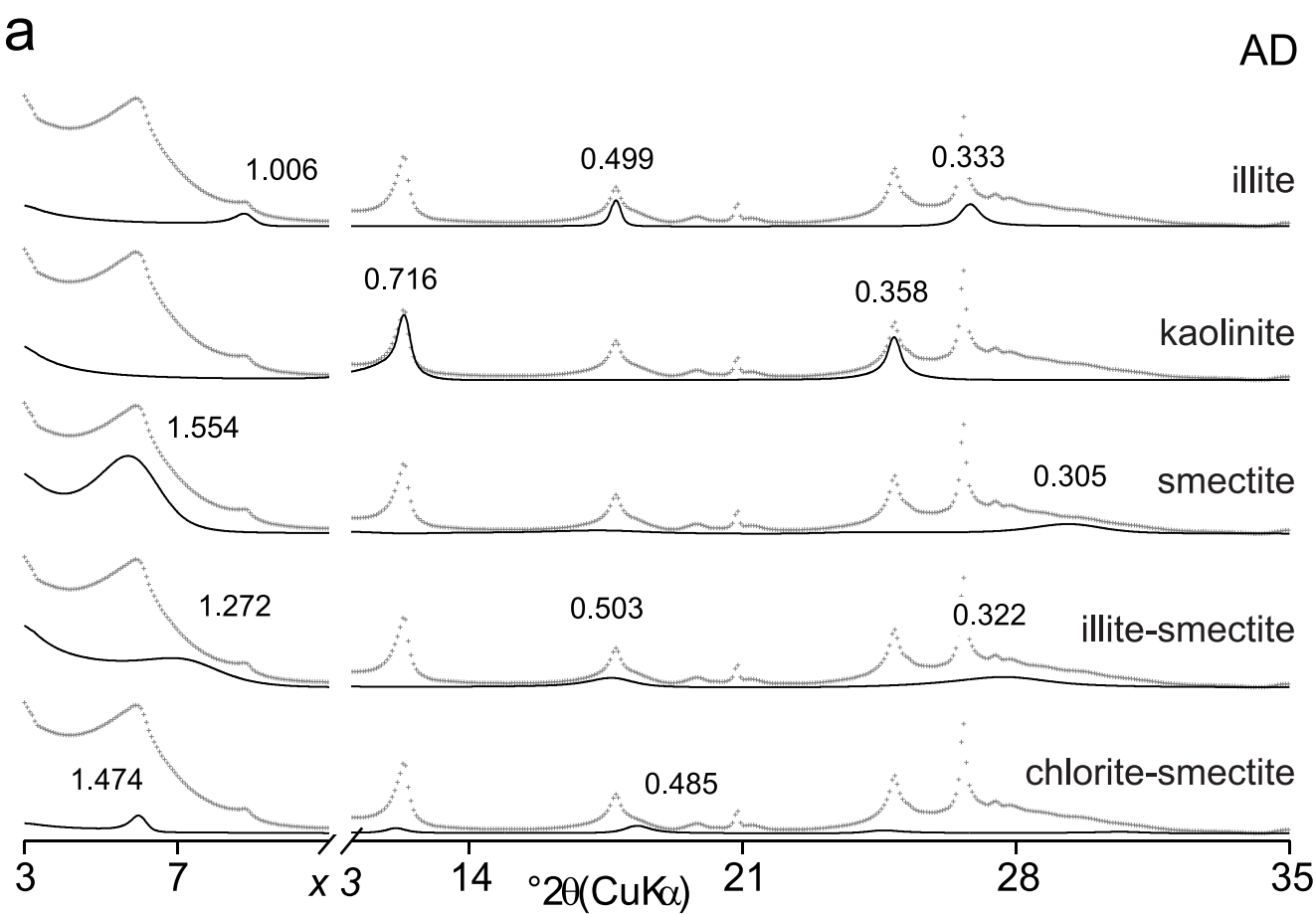
4 AD: Results obtained on the air-dried preparation

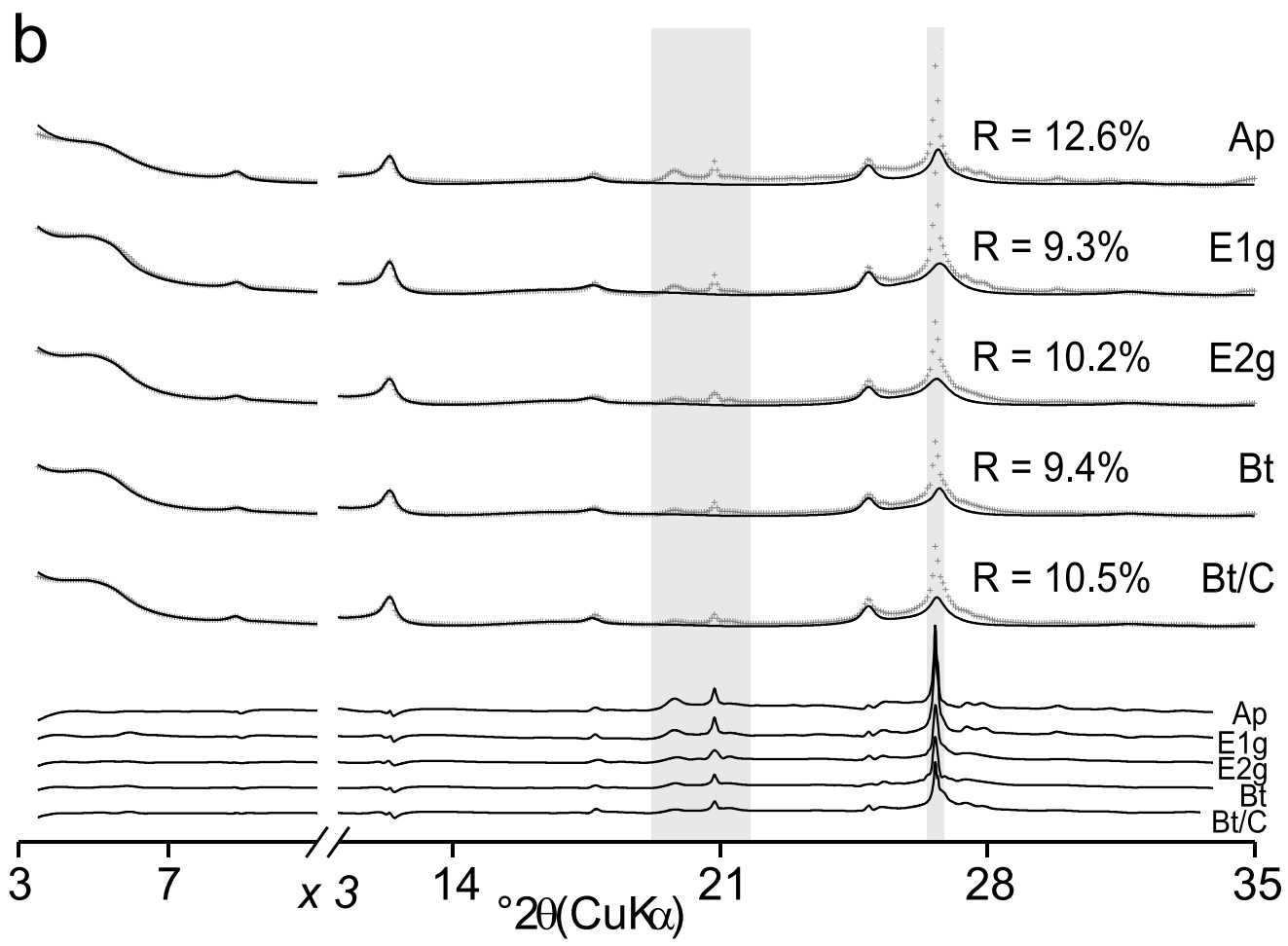
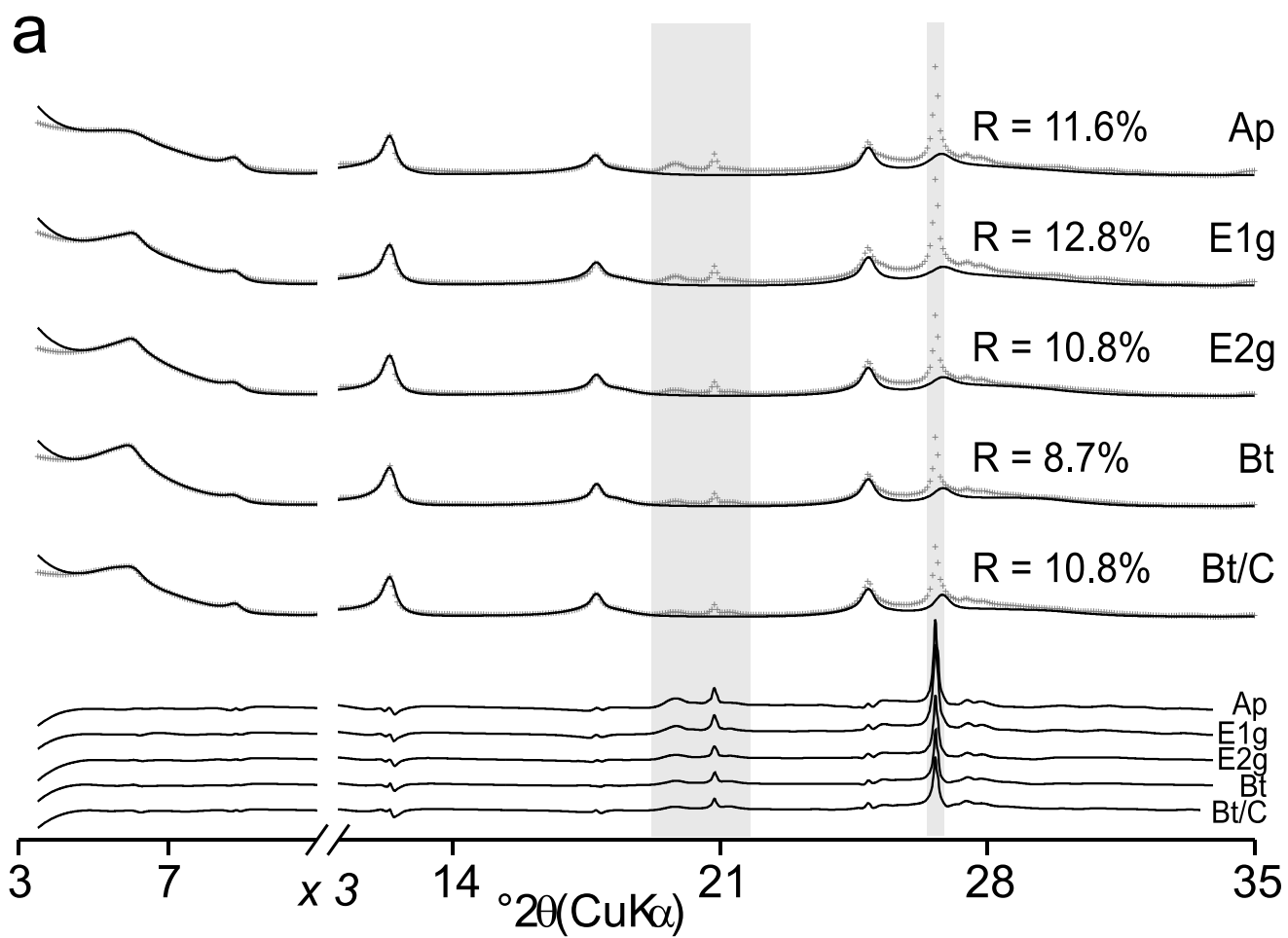
5 EG: Results obtained after ethylene glycol solvation



AD**EG****Ap****E1g****E2g****Bt****Bt/C**







Bt (AD)

